Interlayer coupling between Fe3O4 layers separated by an insulating nonmagnetic MgO layer

Interlayer coupling between Fe_3O_4 layers separated by an insulating nonmagnetic MgO layer

P. A. A. van der Heijden, P. J. H. Bloemen,* and J. M. Metselaar
Department of Physics, Eindhoven University of Technology (EUT), 5600 MB Eindhoven, The Netherlands

R. M. Wolf, J. M. Gaines, J. T. W. M. van Eemeren, and P. J. van der Zaag
Philips Research Laboratories, Prof. Holstlaan 4, 5656 AA Eindhoven, The Netherlands

W. J. M. de Jonge
Department of Physics, Eindhoven University of Technology (EUT), 5600 MB Eindhoven, The Netherlands
(Received 19 July 1996)

The magnetic interlayer coupling between two magnetic layers separated by an insulator was investigated on $Co_{0.2}Fe_{2.8}O_4/Fe_3O_4/MgO/Fe_3O_4$ samples grown by means of molecular beam epitaxy on (001) $MgAl_2O_4$ substrates. The samples were designed to observe interlayer coupling of either sign. Hysteresis loop measurements show that the Fe_3O_4 layers are ferromagnetically coupled in the thickness range 0–45 nm MgO. Below a MgO spacer thickness of 1.3 nm, the coupling strength increases drastically with decreasing MgO thickness and is ascribed to the existence of ferromagnetic bridges through the MgO spacer. The small ferromagnetic coupling above 1.3 nm seems to arise from a magnetostatic coupling due to correlated interface irregularities. [S0163-1829(97)07017-3]

I. INTRODUCTION

Since the discovery that two magnetic layers separated by a nonmagnetic spacer can be coupled ferro- or antiferromagnetically, this phenomenon has been studied extensively, although mostly in entirely metallic systems.[1] So far, studies on interlayer exchange coupling between metallic magnetic layers separated by nonmetallic interlayers, i.e., semiconductors or insulators, are scarce. In an entirely oxidic system, Fe_3O_4/NiO multilayers, an indication for coupling of the magnetite (Fe_3O_4) layers across NiO was found for thicknesses below 5 nm, which was believed to be related to the antiferromagnetism of NiO.[2]

Slonczewski proposed a theoretical model according to which spin-polarized conduction electrons of semi-infinite one- or two-band metallic magnetic layers tunnel from one layer to another across a nonmagnetic insulating interlayer.[3] As a result of this spin-polarized tunneling, an effective Heisenberg-like interlayer coupling between the magnetizations of the magnetic layers across a nonmagnetic insulator was predicted. The coupling is either ferromagnetic or antiferromagnetic and the strength decreases rapidly with increasing interlayer thickness (quicker than exponentially).

The purpose of this study is to determine the interlayer coupling of magnetite layers across a spacer of MgO, which is both insulating and nonmagnetic. Samples composed of a stack of $Co_xFe_{3-x}O_4/Fe_3O_4/MgO/Fe_3O_4$ layers were grown on (001) $MgAl_2O_4$ single-crystal substrates. The MgO spacer layer was either of uniform thickness or in the form of a wedge. The purpose of the $Co_xFe_{3-x}O_4$ base layer was to increase the coercive field of the Fe_3O_4 layer grown on top of it with respect to the second Fe_3O_4 layer. This enables one to distinguish the two Fe_3O_4 layers magnetically and to quantify both ferromagnetic and antiferromagnetic coupling.

II. EXPERIMENT

A. Growth

Samples were grown using a differentially pumped UHV Balzers UMS 630 multichamber molecular beam epitaxy system (MBE) equipped with electron beam evaporators for the Fe and Co targets and a Knudsen cell for Mg. Oxygen was supplied through a ring-shaped doser located close to the substrate. Before and during the deposition, the atomic fluxes were controlled by a crossbeam quadrupole mass-spectrometer feedback system. The layers were deposited at a rate of 0.02–0.05 nm/s, at a substrate temperature of 500 K in an ambient oxygen atmosphere of 3 mPa. More details on the preparation can be found elsewhere.[4]

Two wedge-type samples consisting of a MgO spacer deposited in the form of a wedge and one uniform sample were grown on (001) $MgAl_2O_4$ substrates. One wedge-type sample was composed of a stack of 33 nm $Co_{0.17}Fe_{2.83}O_4$/32.5 nm Fe_3O_4/MgO wedge from 0 to 8.3 nm/21.5 nm Fe_3O_4. The second wedge-type sample was composed of 30 nm $Co_{0.2}Fe_{2.8}O_4$/30 nm Fe_3O_4/MgO wedge from 2 to 45 nm/20 nm Fe_3O_4. The uniform sample was composed of a stack of 27.5 nm $Co_{0.2}Fe_{2.8}O_4$/30 nm Fe_3O_4/5 nm MgO/20 nm Fe_3O_4. A schematic picture of the wedge-type sample described first is given in Fig. 1. The MgO wedge was deposited such that it covered only part of the bottom bilayer. Also the top Fe_3O_4 layers was grown on a limited part of the sample area. This sample design enabled independent investigation of the magnetic behavior of the bottom and top magnetic layers.

As we will show, the use of a (001) $MgAl_2O_4$ substrate yields relaxed ferrite layers due to the large lattice mismatch of -4% between the ferrite layers and the (001) $MgAl_2O_4$ substrate. No (001) MgO substrates were used, although this results in pseudomorphic growth of the multilayer (the lattice mismatch is only 0.3%) and in addition yields a higher struc-

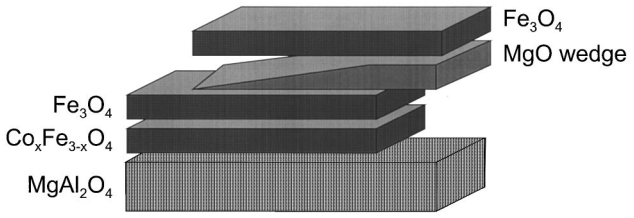

FIG. 1. Schematic representation of a wedge-type sample used in the MOKE studies. The relative shift of the 33 nm $Co_xFe_{3-x}O_4$/32.5 nm Fe_3O_4 bilayer with respect to the top 21.5 nm Fe_3O_4 layer allows the identification of the individual magnetic contributions. The thickness of the MgO wedge varied between 0 and 8.3 nm.

tural quality. However, the tensile strain accompanying the pseudomorphic growth is undesirable in this case because it leads to a perpendicular magnetization orientation for the $Co_xFe_{3-x}O_4/Fe_3O_4$ bilayer due to the large negative magnetoelastic constant of $Co_xFe_{3-x}O_4$.[5,6] The magnetization of the top Fe_3O_4 layer will be oriented in the film plane due to the shape anisotropy. Two different preferential orientations for the magnetization of the magnetic layers would unnecessarily complicate the analysis.

In situ reflection high energy electron diffraction (RHEED) experiments indicated epitaxial growth of each individual layer. During the $Co_xFe_{3-x}O_4$ and Fe_3O_4 growth, the RHEED pattern characteristic of a reconstructed spinel structure[7] was observed. The deposition of MgO resulted in a RHEED pattern characteristic for the rocksalt structure.

X-ray diffraction measurements with the scattering vector perpendicular to the layer planes performed on the uniform sample showed a (001) texture. The measured perpendicular lattice constant of the multilayer peak was 0.840 nm. The lattice constant of the oxygen lattice of the $Co_xFe_{3-x}O_4$, Fe_3O_4 and MgO layers differs very little compared to the -4% lattice mismatch with the $MgAl_2O_4$ substrate.[8] Therefore, one might expect that the lattice of the multilayer acts as one layer and a strain relaxation occurs at the $MgAl_2O_4/Co_xFe_{3-x}O_4$ interface. The observed value of 0.8400 nm is close to the bulk lattice constants of Fe_3O_4 and $CoFe_2O_4$, 0.8396 and 0.8381 nm, respectively,[8] and therefore the $Co_xFe_{3-x}O_4$ layer seems to be relaxed for the present samples. Consequently, the use of a (001) $MgAl_2O_4$ substrate results in a magnetoelastic anisotropy contribution for the $Co_xFe_{3-x}O_4$ layer which is zero or, if any compressive strain is present, favors an in-plane magnetization direction of the $Co_xFe_{3-x}O_4/Fe_3O_4$ bilayer. As explained before, this is desirable for the magnetic coupling study.

B. Magnetic characterization

The temperature-dependent magnetic characterization of the uniform sample was performed using a SQUID magnetometer (Quantum Design, MPMS5). The wedge-type sample was investigated using the magneto-optic Kerr effect (MOKE) with a HeNe laser beam ($\lambda = 633$ nm) as well as a diode laser (Philips, CQL78440/D, $\lambda = 784$ nm) at room temperature. Local MOKE measurements were used to investigate the thickness dependence of the interlayer coupling in a similar fashion as done in, for example, Ref. 9. The spot size

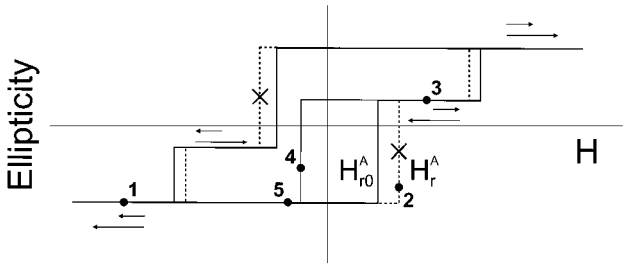

FIG. 2. Schematic hysteresis loop for two magnetic layers with different coercive fields measured by means of MOKE. The largest contribution to the ellipticity originates from the top magnetic layer with the smallest coercive field and magnetic moment. The small and large arrows indicate the magnetization direction of the magnetic layers. In the case of decoupled magnetic layers, the observed hysteresis loop is given by the solid line. The hysteresis loop in the case of (a small degree of) ferromagnetic coupling between the magnetic layers is given by the dotted curve; see text. The magnetization process shown by the numbers is associated with a minor loop measurement; see text. The crosses denote the positions in the hysteresis loop from which the reversal field of the magnetic layer with a low reversal field, H_r^A, is determined.

of 175 μm for the HeNe laser beam at the sample and the two wedge slopes of 0.9 and 3 nm/mm, respectively, yield a resolution of 0.16 and 0.53 nm MgO layer thickness for the wedge-type samples with maximum MgO spacer thicknesses of 8.3 and 45 nm, respectively. The MOKE studies were performed in the longitudinal geometry with the field applied along in-plane [110] and [100] directions.

C. Modeling

The sign (ferro or antiferro) and strength of coupling between two magnetic layers across a nonmagnetic interlayer can be measured by the hysteresis loop if both magnetic layers have different coercive fields. In the case of zero magnetic coupling between the two magnetic layers, a stepped hysteresis loop will be observed due to the different coercive fields of the magnetic layers. The steps correspond to the two coercive fields; see, e.g., Fig. 2 (solid curve). Coupling between the magnetic layers will result in a change of the external field at which the magnetization of each layer reverses its orientation. In the case of (anti)ferromagnetic coupling, the (anti)parallel alignment of the magnetization of the magnetic layers is stabilized and the field interval at which the magnetizations of the magnetic layers are antiparallel aligned (increases) decreases; see, e.g., Fig. 2 (dotted curve for small ferromagnetic coupling). The shift of the reversal fields of the magnetizations can be determined by either measuring a major hysteresis loop, in which case the reversal fields of both layers can be observed, or by measuring a minor loop which is only possible for the layer with the smallest coercive field. An example of an minor loop measurement is shown in Fig. 2: After saturation of the magnetizations of both magnetic layers by a large negative field (point 1 in Fig. 2), the field is increased up to a value (point 3) at which the magnetization of only one layer is reversed (point 2). Subsequently, the external field is decreased to a negative value (point 5) at which the magnetization of the layer is reversed back towards its original position (point 4). If one assumes a

single magnetic domain in each magnetic layer with magnetizations only parallel or antiparallel to the applied field, analytical expressions for the exchange coupling constant, J, in terms of the reversal fields can be derived. Equating the coupling energy density (J/t) and the Zeeman energy density difference between the stepped hysteresis loops in the absence and presence of interlayer coupling, one obtains[10]

$$J=(H_r^A-H_{r0}^A)\mu_0 t^A M_s^A \tag{1a}$$

$$=(H_{r0}^B-H_r^B)\mu_0 t^B M_s^B. \tag{1b}$$

The superscripts, A and B, refer to the two magnetic layers with low and high reversal fields, respectively. The thickness and saturation magnetization of the magnetic layers are denoted by t^i and M_s^i, respectively, with $i=A, B$. The field H_r^i (H_{r0}^i) is the field at which the magnetization of the magnetic layer i reverses its orientation in the presence (absence) of interlayer coupling when varying the applied field from highly negative to positive values. If, instead of a major loop, a minor loop is measured after the saturation of the magnetizations of both magnetic layers by a large negative field (see Fig. 2), one can replace $(H_r^A-H_{r0}^A)$ in Eq. (1a) by the field around which the minor loop is centered, H_{shift}. With increasing ferromagnetic coupling the field interval at which the magnetizations are antiparallel aligned decreases, until the ferromagnetic coupling is so strong that the magnetizations of the layers simultaneously reverse their orientations and a single square hysteresis loop is observed. Then the reversal field of the single square hysteresis loop is obtained by equating 1(a) and 1(b) and taking $H_r=H_r^A=H_r^B$:

$$H_r=\frac{t^A M_s^A H_{r0}^A+t^B M_s^B H_{r0}^B}{t^A M_s^A+t^B M_s^B}. \tag{2}$$

As we stated before, the expressions above hold in the case of a single magnetic domain in each layer and the magnetization of each layer (anti)parallel to the applied field. The assumption of a single magnetic domain in each magnetic layer will hold if the domain wall energy of the magnetic layer is large compared to the coupling energy or if the domain wall width is larger than the thickness of the magnetic layer. The domain wall energy of magnetite is calculated to be 1.65 mJ/m^2 and the domain wall width about 65 nm at room temperature. The other assumption of an (anti)parallel alignment of the magnetization to the applied field holds if the hysteresis loop is measured along an easy magnetization axis of both magnetic layers and the anisotropy of at least one magnetic layer is much larger than J/t. We will show later on that both assumptions are fulfilled in the present experiments.

III. RESULTS AND DISCUSSION

A. Uniform sample at room temperature

Figure 3 shows hysteresis loops obtained by SQUID magnetometry at room temperature for the uniform sample composed of 27.5 nm $Co_xFe_{3-x}O_4$/30 nm Fe_3O_4/5 nm MgO/20 nm Fe_3O_4 ($x = 0.20$). The two loops correspond to measurements with the field applied along [110] and [100] in-plane directions. The magnetization curves are a superposition of two hysteresis loops with different reversal fields and magnetic moment. From an inner loop measurement, the obtained normalized saturation magnetic moment of the top Fe_3O_4 layer is 485 kA/m, which is within the experimental accuracy the bulk value of 496 kA/m[8]. From the data on the wedge-shaped sample [Figs. 4(a) and 4(e), which will be discussed later], we can discriminate the contributions of the thin Fe_3O_4 top layer and the $Fe_3O_4/Co_{0.2}Fe_{2.8}O_4$ bilayer. The hysteresis loop with the lowest reversal field of 22 kA/m arises from the 20 nm Fe_3O_4 top layer and is responsible for the smallest magnetic contribution in the measurement of Fig. 3 with the field applied along a [110] direction. The $Co_xFe_{3-x}O_4/Fe_3O_4$ bilayer acts as a magnetic entity with a reversal field of about 60 kA/m. This relatively large value compared to that of the single Fe_3O_4 top layer is caused by the high coercivity of $Co_xFe_{3-x}O_4$,[11] which, when strongly ferromagnetically coupled to the Fe_3O_4 layer, enhances the effective coercive field of the bilayer [see Eq. (2)].

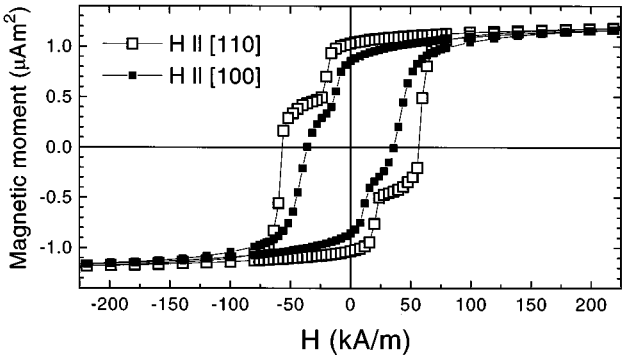

FIG. 3. The hysteresis loops obtained at 300 K of the uniform sample 20 nm Fe_3O_4/5 nm MgO/30 nm Fe_3O_4/27.5 nm $Co_{0.2}Fe_{2.8}O_4$ grown on (001) $MgAl_2O_4$. The two loops correspond to measurements with the field applied along [100] and [110] in-plane directions (1 kA/m = 4π Oe).

To simplify the quantification of the exchange coupling strength using Eqs. (1a) and (1b), the magnetization measurement has to be performed along an easy magnetization axis of the magnetic layers. From the remanence of the hysteresis loops shown in Fig. 3, it is concluded that for both magnetic layers, the ⟨110⟩ in-plane axes are the easy magnetization axes. The in-plane easy magnetization axes are determined by the magnetocrystalline anisotropy. Based on literature values for bulk $Co_xFe_{3-x}O_4$,[8,12] one would expect that the Co-ferrite layer would dominate the in-plane anisotropy of the $Fe_3O_4/Co_{0.2}Fe_{2.8}O_4$ bilayer, which, in contrast to the observation, would result in an ⟨100⟩ in-plane easy magnetization axis. It is well known that the in-plane anisotropy of thin films can be altered at the surface (interface) of the film. The discrepancy in the magnetocrystalline anisotropy between the bulk and our MBE-grown Co-ferrite thin film might arise from an altered surface (interface) contribution. Another possible explanation for the observed discrepancy might be a difference in Co and Fe cation distributions over the octahedral and tetrahedral sites between the bulk and MBE-grown material, which could alter the magnetocrystalline anisotropy of the whole layer.

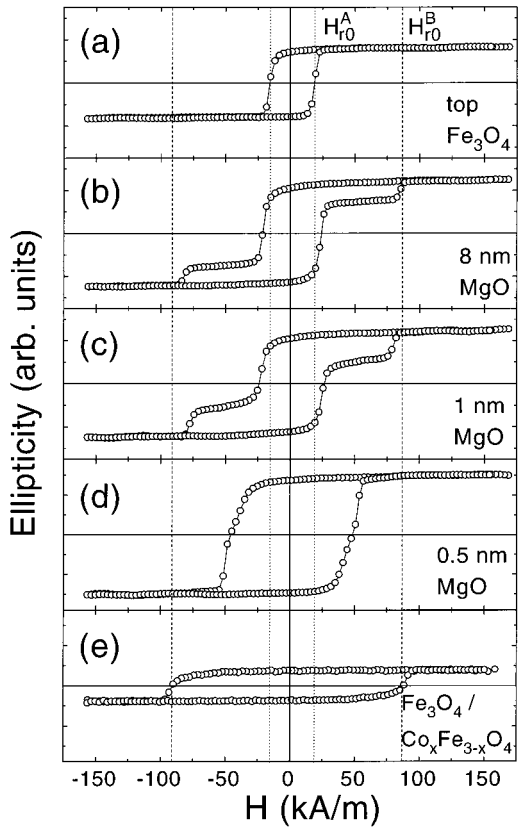

FIG. 4. Examples of hysteresis loops at different positions on a wedge-type sample measured in the longitudinal MOKE geometry with the field applied along a [110] direction. The positions on the sample correspond to: (a) only the top Fe_3O_4/MgO layer (right side of sample), the entire multilayer at MgO interlayer thicknesses of (b) 8 nm , (c) 1 nm, and (d) 0.5 nm, and (e) only the bottom $Co_xFe_{3-x}O_4/Fe_3O_4$ bilayer (x=0.17) (left side of sample). All MOKE measurements have been performed with a 633 nm laser, with the exception of (e) where a 784 nm laser was used.

B. Thickness dependence of the interlayer coupling

The wedge-type samples were used to investigate the exchange coupling constant at room temperature as a function of the MgO spacer thickness. Figure 4 shows characteristic hysteresis loops observed at different positions on the sample shown in Fig. 1 with the field applied along a preferential [110] direction. Figures 4(a) and 4(e) show the hysteresis loops obtained from the right and left sides of the sample, respectively, as shown in Fig. 1. These hysteresis loops identify the individual magnetic behavior of the top 21.5 nm Fe_3O_4 layer and the 32.5 nm $Co_xFe_{3-x}O_4$/32.5 nm Fe_3O_4 bilayer. The hysteresis loop with a small coercive field originates from the top Fe_3O_4 layer and the hysteresis loop with the high coercive field originates from the $Co_xFe_{3-x}O_4/Fe_3O_4$ bilayer. Figures 4(b) and 4(c) show characteristic examples of stepped hysteresis loops obtained for MgO spacer thicknesses above 1 nm. The reversal fields of the soft (top Fe_3O_4) and hard ($Co_xFe_{3-x}O_4/Fe_3O_4$) layers are close to the values obtained from Figs. 4(a) and 4(e), respectively, which indicates small magnetic coupling. For small MgO spacer thicknesses, however, a square hysteresis loop is measured implying strong ferromagnetic coupling; see, e.g., Fig. 4(d).

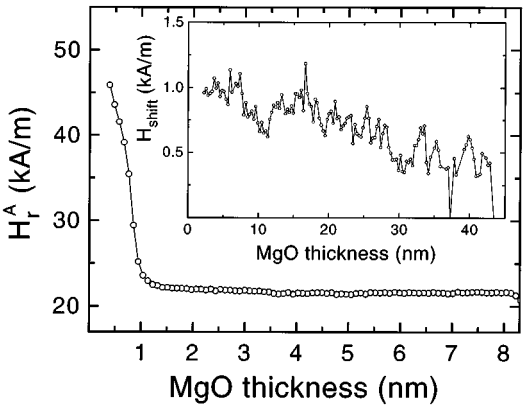

FIG. 5. The main figure shows the reversal fields of the 21.5 nm Fe_3O_4 layer vs the MgO interlayer thickness for the wedge-type sample shown in Fig. 2. The inset shows the MgO spacer thickness dependence of the shift of the minor loop for the 20 nm Fe_3O_4 layer, H_{shift}, obtained from the wedge-type sample with the MgO thickness varied between 2 and 45 nm. The minor loops are measured after the saturation of the magnetization of the both layers by applying a large negative field.

Before proceeding with the analysis, we want to point out that the behavior of the magneto-optical properties observed for the bottom $Co_xFe_{3-x}O_4/Fe_3O_4$ bilayer is rather anomalous. We found that the magnitude of the Kerr ellipticity of the uncovered bilayer becomes zero using a 633 nm wavelength laser. The disappearance of the Kerr ellipticity at 633 nm in the uncovered case may be explained by assuming a Kerr ellipticity for these ultrathin Fe_3O_4 and $Co_xFe_{3-x}O_4$ layers, which are equal in magnitude but opposite in sign. A wedge on top of the bilayer can alter the relative contributions of the individual layers, which in this case apparently leads to a nonzero Kerr ellipticity [see Figs. 4(b), 4(c), and 4(d)]. The magnitude of the Kerr ellipticity of these materials depends strongly on the wavelength and specific chemical composition.[13,14] This is illustrated by the fact that at $\lambda = 784$ nm the Kerr ellipticity for the uncovered bilayer was nonzero [Fig. 4(e)].

From Fig. 4 it appears that in the presence of the MgO wedge, the contribution to the Kerr ellipticity of the Fe_3O_4 top layer is about twice that of the bottom bilayer. Therefore, the applied field at which the Kerr ellipticity is one-third of the saturation ellipticity in the stepped hysteresis loop is equal to the field at which the magnetization of the 21.5 nm Fe_3O_4 top layer reverses its orientation, H_r^A (indicated by a cross in Fig. 2). The results obtained for H_r^A in this manner are shown in the main figure of Fig. 5 for the wedge-type sample with the MgO spacer thickness varied between 0 and 8.3 nm. We checked that small variations in the magnitude of the ellipticity, at which H_r^A is defined, do not alter the observed thickness dependence of H_r^A significantly. We remark that data for H_r^B are not used to quantify the exchange coupling constant, because the variations in H_r^B are smaller than in H_r^A due to the large magnetic moment of the bottom bilayer, which results in a larger error in the determination of J.

Two thickness ranges corresponding to different coupling regimes can be discerned (Fig. 5). At MgO thicknesses

above 1.3 nm, H_r^A decreases gradually with increasing MgO spacer thickness. In this case the magnetite layers are weakly coupled and a clear field interval at which the magnetization of both magnetic layers are antiparallel aligned is observed, which enable an accurate measurement of a minor loop of the soft-magnetite layer. The minor loops measured after saturation of the magnetization of both magnetic layers by a large negative field are shifted from zero to positive applied fields implying ferromagnetic coupling. The inset of Fig. 5 shows the MgO spacer thickness dependence of the shift of the minor loop, H_{shift}, obtained from the wedge-type sample with a maximum MgO thickness of 45 nm. The gradual decrease of H_{shift} with increasing MgO spacer thickness implies a gradual decreasing ferromagnetic coupling. At MgO thicknesses below 1.3 nm, H_r^A shown rapidly increases implying a rapid increasing ferromagnetic coupling and we are apparently in a different coupling regime. Below a spacer thickness of 0.8 nm MgO, the strong ferromagnetic coupling results in a square hysteresis loop with a reversal field between the reversal fields of the decoupled Fe_3O_4 top layer and the $Co_xFe_{3-x}O_4/Fe_3O_4$ bilayer [Fig. 4(d)]. Although the hysteresis loop is square, H_r^A still increases with decreasing MgO spacer thickness. The reversal field of the square hysteresis loop extrapolates to 60 ± 6 kA/m for vanishing MgO thicknesses. This is close to the value 71 kA/m, obtained from Eq. (2) using the value $H_{r0}^A = 18.7$ kA/m and $H_{r0}^B = 89$ kA/m derived from Figs. 4(a) and 4(e).

The exchange coupling constant at the several MgO thicknesses can be calculated straightforwardly using Eq. (1a). For small MgO spacer thicknesses, J has been calculated from the reversal field, H_r^A, shown in Fig. 5 with $t = 21.5$ nm, $\mu_0 M_s = 0.62T$,[8] and $H_{r0}^A = 18.7$ kA/m. For large MgO spacer thicknesses, J has been calculated from the shift of the minor loop by replacing $(H_r^A - H_{r0}^A)$ in Eq. (1a) by H_{shift} (shown in the inset of Fig. 5), and using $t = 20$ nm. Figure 6 shows this thickness dependence of J for the MgO spacer thickness intervals of 0.4–1.4 and 2–45 nm (open and solid circles). Here, the solid lines represent calculations to be discussed later. The maximum value for J of 0.22 mJ/m^2 found (see Fig. 6) is an order of magnitude smaller than the domain wall energy of 1.65 mJ/m^2 and therefore one can assume a single magnetic domain in the magnetic layers, which was a first condition for the application of Eq. (1). The second condition which concerns the alignment of the moments to the applied field is apparently fulfilled since we are observing square loops. This behavior is probably induced by the large anisotropy of the bottom bilayer since a comparison of J/t and the anisotropy of the magnetite top layer indicates the same order of magnitude.

Three possible origins for the observed coupling behavior will be discussed, namely, coupling due to tunneling, ''pinholes,'' and a magnetostatic effect. The model mentioned in the introduction in which magnetic layers separated by a nonmagnetic insulator could couple either ferro- or antiferromagnetically with the coupling strength decreasing rapidly with increasing interlayer thickness[3] seems to explain the experimental data at small thicknesses of the MgO spacer. However, quantitative interpretation of the data for the thickness dependence of the coupling strength in terms of the tunneling model is difficult. The theory is based on *metallic*

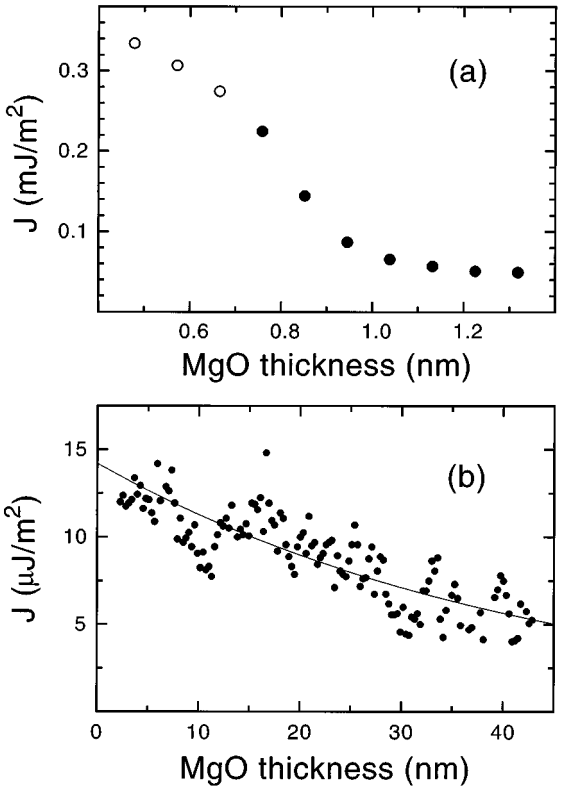

FIG. 6. The thickness dependence of the interlayer exchange coupling constant, J, calculated from (a) the change in the reversal field of the top 21.5 nm Fe_3O_4 layer and (b) the shift of the minor loop of the top 20 nm Fe_3O_4 layer. The data represented by the open circles in (a) are obtained from square hysteresis loops and are therefore an underestimation of the coupling strength. The solid line in (b) represent the fit to the data using an ''orange peel'' type of magnetostatic coupling, Eq. (3).

magnetic layers whereas magnetite is an *oxide* in which the conduction is of hopping type. Therefore, the applicability of the model using a band structure of magnetite is doubtful. Furthermore, the interpretation of the observed coupling in terms of the tunneling mechanism is also complicated by the existence of an interface region in the Fe_3O_4 layer with a negligible electrical conductivity and an apparent loss of magnetization.[15,16] The origin of this interface region is believed to arise from a disordered spin structure, which will influence the spin asymmetry in the tunneling probability. Although, the possibility of a tunneling mechanism giving rise to the observed ferromagnetic coupling cannot be excluded, the observation of ferromagnetic instead of antiferromagnetic coupling offers the possibility for alternative mechanisms.

It is therefore possible that the strong ferromagnetic coupling observed for low MgO spacer thicknesses could originate from pinholes due to interface roughness, which give rise to magnetic bridges through the nonmagnetic spacer. To investigate the interface roughness, STM measurements were performed on a 40 nm Fe_3O_4 layer grown on (001) MgO. These measurements showed that the Fe_3O_4 surface consists of terraces with a typical lateral length of several tens of nanometers.[17] Adjacent terraces were separated by single steps with a vertical height of one to four oxygen planes

(0.21–0.84 nm). This implies that the deposition of a MgO layer up to 0.84 nm thick is insufficient to fully cover the Fe_3O_4 surface and to isolate the Fe_3O_4 layer grown on top of MgO from the Fe_3O_4 layer below. The samples in this study can be expected to be rougher than those in the STM study, because of the larger lattice mismatch (-4%) between Fe_3O_4 and the $MgAl_2O_4$ substrate. The magnetic data showing strong coupling below a MgO spacer thickness of 1.3 nm suggest the presence of pinholes up to 1.3 nm also indicating an increased interface roughness for the present samples.

The small ferromagnetic coupling observed above a MgO spacer thickness of 1.3 nm may be due to ''orange peel'' type of magnetostatic coupling. This magnetostatic coupling between two magnetic layers originates from magnetic charges localized at each interface due to structural irregularities at the interface.[18] The coupling is ferromagnetic in the case the roughness of the surface at the start of MgO growth propagates to the top of the MgO layer, which produces correlated interface topography of both magnetite layers. In the case of two identical magnetic layers with a uniform magnetization rigidly directed along an easy axis and an interface roughness, σ, periodic in the two lateral directions x and y with period $2\pi/p$ and a height variation h [$\sigma = h\sin(px)\sin(py)$], the coupling strength, J, is given by[18]

$$J = \frac{1}{2\sqrt{2}} \pi p h^2 \mu_0 M_s^2 e^{-p\sqrt{2}d}, \tag{3}$$

where d is the spacer thickness. The fit of Eq. (3) for J to data in the MgO interlayer thickness interval of 2–45 nm is shown by the solid line in Fig. 6(b). The roughness parameters obtained from the fit are $2\pi/p = (39 \pm 2) \times 10$ nm and $2h = 3.1 \pm 0.1$ nm. The obtained ratio for the height fluctuation per length unit of $2h/(\pi/p) = 3.1/195 = 0.016 \pm 0.001$ is close to the ratio of about 0.012 obtained from the estimation of the average step height (0.3 nm) and terrace length (25 nm) of the STM measurements[17] taken into account the difference between the interface roughness of the sample used for the STM study and the present samples. Therefore the small ferromagnetic coupling observed above a spacer thickness 1.3 nm MgO is consistent with magnetostatic coupling and the known interface roughness.

C. Temperature dependence of the interlayer coupling

To substantiate that the observed ferromagnetic coupling for large MgO spacer thicknesses is due to an ''orange peel'' type of magnetostatic coupling, the temperature dependence of the interlayer exchange coupling constant has been investigated for the uniform sample. Figure 7 shows the temperature dependence of the interlayer exchange coupling constant, J, obtained from minor loop measurements and the square of the magnetic moment of the sample. According to Eq. (3), the coupling strength is proportional to the square of the magnetization of the two identical magnetic layers. Figure 7 shows that the square of the magnetic moment only slightly increases with decreasing temperature, which can be expected in the temperature regime of 0–300 K for magnetic layers with relative high Curie temperatures (860 and 790 K for Fe_3O_4 and $CoFe_2O_4$, respectively). Figure 7 shows that the temperature dependence for J and the square of the magnetic moment are within the experimental accuracy identical, which is expected for an ''orange peel'' type of magnetostatic coupling between the magnetite layers, see Eq. (3). Note that the large scatter of the exchange coupling constant in Fig. 7 is due to the relative large coercive field of the top Fe_3O_4 layer compared to the shift of the minor loop, e.g., the coercive field is about 1000 Oe at 5 K while H_{shift} is only 25 Oe.

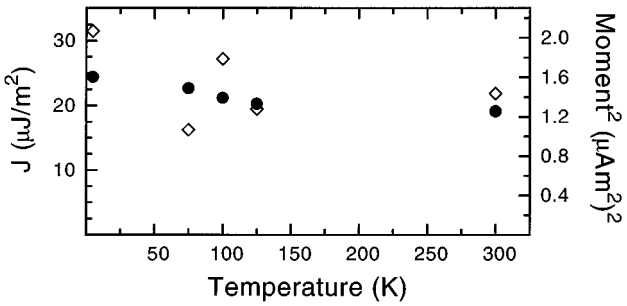

FIG. 7. The temperature dependence of the interlayer exchange coupling constant, J (open diamonds, left axis) and square of the magnetic moment (solid circles, right axis) of the uniform sample 20 nm Fe_3O_4/5 nm MgO/30 nm Fe_3O_4/27.5 nm $Co_{0.2}Fe_{2.8}O_4$ grown on (001) $MgAl_2O_4$.

IV. CONCLUSIONS

The study of interlayer coupling of magnetite layers across a MgO spacer for a thickness range 0–45 nm MgO showed that the coupling between the magnetite layers is always ferromagnetic and small at MgO thicknesses above 1.3 nm. Below 1.3 nm MgO, the ferromagnetic coupling increases drastically with decreasing MgO interlayer thickness. Reliable values for the magnitude of the coupling strength can be determined for MgO spacer thicknesses above 0.8 nm. At 0.8 nm, the exchange coupling constant is estimated to be 0.22 mJ/m^2. Below 0.8 nm, the ferromagnetic coupling strength increases further. We suggest that coupling below MgO spacer thicknesses of 1.3 nm is dominated by ferromagnetic bridges between the magnetite layers arising from large single steps between adjacent terraces of the magnetite surface. The coupling for spacer thicknesses above 1.3 nm can be described as magnetostatic coupling due to correlated interface irregularities.

ACKNOWLEDGMENTS

We would like to thank J. J. Hammink and M. M. H. Willekens for their assistance in the experiments. Part of this work was supported by the Technology Foundation (STW). The research of P. J. H. Bloemen has been made possible by financial support from the Royal Netherlands Academy of Sciences.

*Present address: Philips Research Laboratories, Prof. Holstlaan 4, 5656 AA Eindhoven, The Netherlands.

[1] *Ultrathin Magnetic Structures I*, edited by B. Heinrich and J.A.C. Bland (Springer-Verlag, Berlin, 1994), Vol. II, and references therein.

[2] J.J. Krebs, D.M. Lind, and S.D. Berry, J. Appl. Phys. **73**, 6457 (1993).

[3] J.C. Slonczewski, Phys. Rev. B **39**, 6995 (1989).

[4] R.M. Wolf, A.E.M. De Veirman, P. van der Sluis, P.J. van der Zaag, and J.B.F. aan de Stegge, in *Epitaxial Oxide Thin Films and Heterostructures*, edited by D. K. Fork, J. M. Phillips, R. Ramesh, and R. M. Wolf, MRS Symposia Proceedings No. 341 (Materials Research Society, Pittsburgh, 1994), p. 23.

[5] R. Leyman and C. Henriet-Iserentant, J. Magn. Magn. Mater. **49**, 337 (1985).

[6] P.J.H. Bloemen, P.A.A. van der Heijden, R.M. Wolf, J. aan de Stegge, J.T. Kohlhepp, A. Reinders, R.M. Jungblut, P.J. van der Zaag, and W.J.M. de Jonge, in *Epitaxial Oxide Thin Films II*, edited by D. K. Fork, J. S. Speck, T. Shiosaki, and R. M. Wolf, MRS Symposia Proceedings No. 401 (Materials Research Society, Pittsburgh, 1996), p. 485.

[7] F.C. Voogt, T. Hibma, G.L. Zhang, M. Hoefman, and L. Niesen, Surf. Sci. **331-333**, 1509 (1995).

[8] V.A.M. Brabers, in *Handbook of Magnetic Materials*, edited by K.H.J. Buschow (Elsevier Science, Amsterdam, 1995), Vol. 8, Chap. 3.

[9] S.T. Purcell, W. Folkerts, M.T. Johnson, N.W.E. McGee, K. Jager, J. aan de Stegge, W.B. Zeper, and W. Hoving, Phys. Rev. Lett. **67**, 903 (1991).

[10] A. Yelon, in *Physics of Thin Films*, edited by M.H. Francombe and R.W. Hoffman (Academic, New York, 1971), Vol. 6, p. 205.

[11] J. Smit and H.P.J. Wijn, *Ferrites* (Philips Tech. Library, Eindhoven, 1959).

[12] R.F. Penoyer and L.R. Bickford, Jr., Phys. Rev. **108**, 271 (1957).

[13] J.W.D. Martens, W.L. Peeters, H.M. van Noort, and M. Erman, J. Phys. Chem. Solids **46**, 411 (1985).

[14] P.J. van der Zaag, W.F.J. Fontijn, P. Gaspard, R.M. Wolf, V.A.M. Brabers, R.J.M. van de Veerdonk, and P.A.A. van der Heijden, J. Appl. Phys. **79**, 5936 (1996).

[15] R.J.M. van de Veerdonk, M.A.M. Gijs, P.A.A. van der Heijden, R.M. Wolf, and W.J.M. de Jonge, *Epitaxial Oxide Thin Films II* (Ref. 6), p. 455.

[16] P.A.A. van der Heijden, P.J.H. Bloemen, J.M. Gaines, J.T.W.M. van Eemeren, R.M. Wolf, P.J. van der Zaag, and W.J.M. de Jonge, J. Magn. Magn. Mater. **159**, L293 (1996).

[17] J.M. Gaines, P.J.H. Bloemen, J.T. Kohlhepp, R.M. Wolf, A. Reinders, R.M. Jungblut, P.A.A. van der Heijden, J.T.W.M. van Eemeren, J. aan de Stegge, W.J.M. de Jonge, and C. Bulle-Lievema, Surf. Sci. (to be published).

[18] L. Néel, Compt. Rendus **255**, 271 (1962); **255**, 1676 (1962).